CHEMISTRY OF MATERIALS

ARTICLE

pubs.acs.org/cm

NO_x Adsorption Site Engineering in Ru/Ba,Na−Y Zeolite

Sylvia Smeekens,[‡] Steven Heylen,[‡] Nikki, Janssens, Kristof Houthoofd, Johan A. Martens, and Christine E. A. Kirschhock*

Centre for Surface Chemistry and Catalysis, Katholieke Universiteit Leuven, Kasteelpark Arenberg 23, 3001 Leuven, Belgium

Supporting Information

ABSTRACT: Adsorption of gas molecules is a typical application for zeolites. Interaction of adsorbed molecules with cations in zeolite frameworks is responsible for selectivity and adsorption strength. Through detailed analysis of the cation distribution in zeolite Y containing Na^+, Ba^{2+}, and Ru^{3+} cations by NMR and X-ray diffraction combined with adsorption studies it was possible to develop a reversible, highly performant NO_x adsorbent. The results demonstrate intimate understanding of guest−host interactions can lead to rational tailoring of zeolite properties.

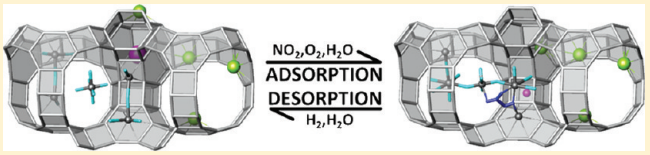

KEYWORDS: Ruthenium, Barium, Zeolite Y, NO_x, Rietveld refinement, cation sites

INTRODUCTION

Modern concepts of NO_x elimination from lean-burn exhaust gases are based on barium compounds trapping NO_x as nitrates.[1−4] NO_x temporarily stored under lean burn conditions is desorbed and reduced to N_2 using a spike of rich gas produced by the engine. The forthcoming EURO 6 legislation imposes very stringent limits on NO_x emissions and is triggering a renewed interest in NO_x traps. Zeolites containing alkali or alkaline earth cations offer great potential in NO_x elimination systems.[5−7] The combination of Ba−Y zeolite with nonthermal plasma has been shown to perform well in selective catalytic NO_x reduction with hydrocarbons.[8−15] In the temperature window 100−177 °C Ba−Y zeolite forms large amounts of nitrate, but decomposition of these nitrates is problematic.[16] However, the functionality of zeolites, porous crystalline aluminosilicates with well-defined cavities and channels, greatly is determined by the positions of the cations balancing the framework charge. Therefore, an optimization of the decoration of the cages of zeolite Y with a specific composition of cations was expected to remedy or even remove the problem of nitrate formation. The here investigated zeolite Y is of faujasite topology (FAU) with a typical framework composition of $Na_{52}Al_{52}Si_{140}O_{384}$ (Figure 1). In general, aluminosilicate zeolites consist of corner sharing oxygen tetrahedra with central Si or Al atoms. The FAU topology can be thought of being assembled from edgewise connected double six rings (D6Rs) (Figure.1). This results in a large and a small cavity system being composed of large supercages (sc) and of sodalite cages (sod), connected via their 12- rings and 6-rings, respectively. Because of the high symmetry of the framework, cations which balance the negative charge caused by the presence of aluminum, mostly occupy well-defined positions.

Depending on the nature and charge of the cations different sites are preferred.[17] A more detailed description of cation sites in FAU can be found in the Supporting Information.

EXPERIMENTAL SECTION

Zeolite Na−Y (Si/Al atomic ratio of 2.7, $Na_{52}Al_{52}Si_{140}O_{384}$ Zeocat) was cation exchanged with an aqueous solution of $BaCl_2.2H_2O$ (≥99+%, Acros) as described in Monticelli et al..[16] After filtration and washing with deionized water, the Ba,Na−Y zeolite was dried in static air at 60 °C. Elemental analysis on this Ba,Na−Y zeolite was performed by ICP-AES (analyzed at Bodemkundige Dienst van België). The unit cell composition corresponded to $Ba_{17.3}Na_{17.3}Al_{52}Si_{140}O_{384}$. An increased Ba content was achieved by a second ion-exchange after calcination at 500 °C for 4 h. Elemental analysis resulted in a unit cell composition of $Ba_{23.5}Na_{5.0}Al_{52}Si_{140}O_{384}$. Ba,Na−Y zeolite was further loaded with ruthenium by suspending 1 g of zeolite powder in 100 mL aqueous solution of $RuCl_3$ (99+%, anhydrous, Acros), and stirring at ambient temperature for 2.5 h. During the loading process, the initial pH was set at 8.5 by addition of ammonia to avoid ruthenium precipitation. Using this procedure, ruthenium in solution was quantitatively taken up by the zeolite as verified via ICP-AES analysis. In the sample notation, the Ru content in wt % is indicated. Ru(0.5%)/Ba,Na−Y is the notation of a Ba, Na−Y zeolite loaded with 0.5 wt % ruthenium. After filtration, washing and drying, the Ru/Ba,Na−Y zeolite was compressed under a hydrostatic pressure of 40 MPa. The compacted tablets were crushed and sieved to obtain pellets of 0.25−0.50 mm for use in an adsorbent bed. X-ray diffraction before and after pelletizing indicated no structural change of the zeolite. Adsorption evaluation was done on a dual-line unit with the adsorbent bed held in a quartz tube as described elsewhere.[18,19] The following standard procedure was applied if not stated differently: the zeolite was heated to 300 °C under a flow of nitrogen containing 5% O_2 and 3% H_2O before NO_x adsorption−desorption cycles were started. Typically the adsorption phase was composed of 1000−1500 ppm NO_x, 5% O_2, 3% H_2O, and balance N_2. It was verified the capacity of the adsorbent did not depend on the NO_x inlet concentration in this

Received: August 1, 2011
Revised: September 12, 2011
Published: September 28, 2011

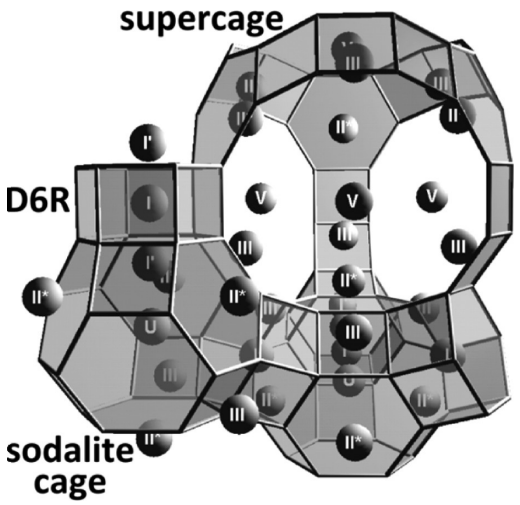

Figure 1. Faujasite topology with indicated double six ring (D6R), sodalite cages (Sod), and supercages and cation positions.

range. Desorption and regeneration of the saturated adsorbent occurred in a N_2 gas flow containing 1% H_2 and 3% H_2O. The gas flow rate was 150 mL STP/min and the catalyst volume 0.6 mL (400 mg), corresponding to a volumetric hourly space velocity (VHSV) of 15,000 h^{-1}. The NO_x concentration at the in- and outlet of the adsorbent bed was analyzed using an internally heated chemiluminescence detector (CLD 700 EL ht, Eco Physics). The NH_3 concentration was measured via UV spectroscopy (Limas 11HW analyzer); N_2O with an Uras 26 NDIR analyzer (both ABB).

X-ray diffraction data were collected on a STOE STADI-P powder diffractometer equipped with a focusing Ge(111)-monochromator and a linear position sensitive detector. All powder samples of the catalysts used in the reactor were sealed in 0.7 mm (outer diameter) glass capillaries (Hilgenberg) under dry nitrogen atmosphere and were measured with Cu $K_{\alpha 1}$-radiation in the range of $4° \leq 2\theta \leq 80°$ in Debye−Scherrer geometry. Asides determination of the crystalline phases, the structure of the Ru/Ba,Na−Y was refined after NO_x ad- and desorption. Samples with a Ru content of 0.5 wt.-% were refined. A higher Ru content leads to the manifestation of of extra-framework Ru phases in the powder patterns, which complicates refinement. Rietveld refinements and difference fourier electron density analyses were performed using the GSAS/EXPGUI software package. The starting model was generated from the structure parameters published by the International Zeolite Association (Web site www.iza-structure.org) and standard cation positions. Cation occupation numbers were constrained to account for the experimentally determined unit cell composition. A more detailed explanation of the refinement strategy and the powder patterns are provided in the Supporting Information.

^{23}Na MAS NMR spectra were recorded on a Bruker Avance DSX400 spectrometer (9.4 T). 5550 scans were accumulated with a recycle delay of 1 s. Samples retrieved from the reactor were packed under inert atmosphere in 2.5 mm rotors. The spinning frequency of the rotor was 20 kHz. Solid NaCl was used as chemical shift reference.

RESULTS AND DISCUSSION

In the initial experiment the adsorption and desorption of NO_x on Ba,Na−Y zeolite with composition $Ba_{17.3}Na_{17.3}Al_{52}Si_{140}O_{384}$ and without transition metal was investigated. The zeolite was found to be inert toward NO. When Ba,Na−Y zeolite, was contacted at 300 °C with gas composed of nitrogen with 1500 ppm NO_2, 3% H_2O, and 5% O_2 considerable NO_2 uptake

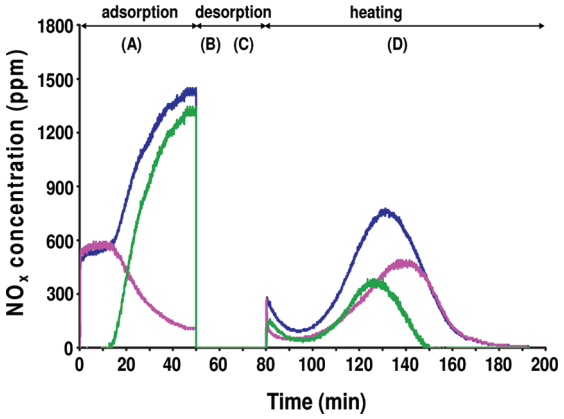

Figure 2. NO_x concentration traces at the adssorber outlet during a NO_x adsorption−desorption cycle of a Ba,Na−Y zeolite at 300 °C: NO_x (blue), NO (pink), NO_2 (green). The Ba,Na−Y zeolite was heated to the adsorption temperature under a flow of 5% O_2, 3% H_2O and balance N_2. During adsorption (A), gas flow was composed as 1500 ppm NO_2, 5% O_2, 3% H_2O and balance N_2. Desorption of NO_x from the adsorbent bed was done with a gas stream with 3% H_2O in N_2 (B). After 10 min desorption, 1% H_2 was added to the gas composition (C). After 30 min desorption (D), the Ba,Na−Y zeolite was heated under N_2 to 450 °C with a ramp of 5 °C/min.

was observed. The reactive adsorption of NO_2 coincided with formation of NO, suggesting nitrate formation according to:

$$3NO_2 + H_2O \rightarrow 2HNO_3 + NO \quad (1)$$

$$M^{+n}\text{-}nZ^- + nHNO_3 \rightarrow M(NO_3)n + n\text{H-Z} \quad (2)$$

as observed in earlier work.[16] After 50 min, the zeolite was saturated with NO_x (Figure 2A). Regeneration at the same temperature using 3% H_2O in a N_2 stream with or without addition of 1% H_2 to the regeneration gas failed (Figure 2B,C). An amount of 20.95 mg NO_x/g eventually was desorbed upon heating to 450 °C under a flow of N_2 (Figure 2D).

A detailed analysis of the positions of cations, water, and NO_x species was expected to reveal strategies to improve the performance of the material. Therefore, the structure of the empty and nitrate saturated Ba,Na−Y zeolite was determined using powder X-ray diffraction and a combination of Rietveld refinement and difference electron density analysis (ESI). Surprisingly, 17 Ba^{2+} cations were located on positions SI′ and SII* inside or in close vicinity to the small cavity system.

This distribution of the doubly charged cations could be rationalized: The presence of one Ba^{2+} on SI′ in 7 of the 8 available sodalite cages (sod) hindered occupation of 3 SII* positions nearby. There remained 4 SII* of the one empty, and one available SII* per occupied sodalite cage. These still accessible SII* sites were found occupied by the 10 remaining Ba^{2+} cations. The synergy between the different cation sites is illustrated in the Supporting Information. Sodium ions usually also prefer occupation of the SII* site. But the presence of Ba^{2+} compelled the Na^+ cations to entirely locate on SIII and SV, where the latter position is far removed from the framework in the center of the windows connecting 2 supercages. Also the sodium on SIII was found farther from the framework as usually encountered, most probably due to the high charge density in the sodalite cage occupied by barium (see Figure 1 in the Supporting Information). Consequently, each Na^+ cation was surrounded by six water molecules

dx.doi.org/10.1021/cm202230r |*Chem. Mater.* 2011, 23, 4606–4611

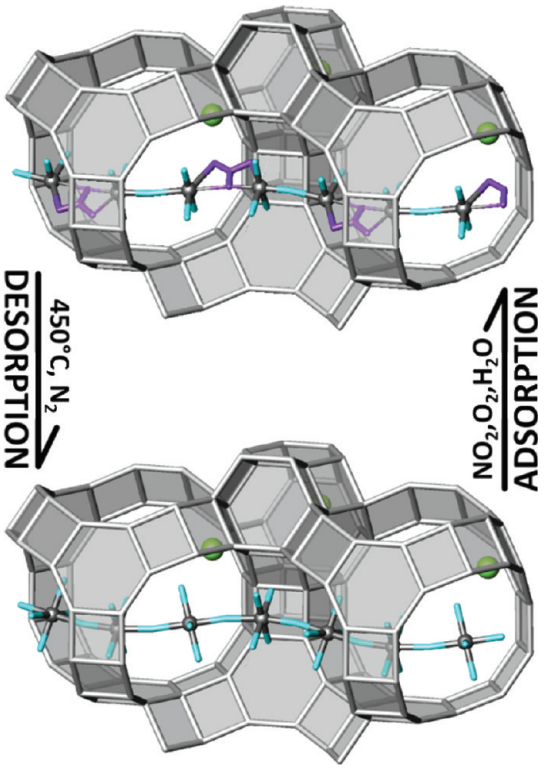

Figure 3. Representation of the nitrate species in the supercages of a NO_x saturated Ba,Na−Y zeolite. The small gray spheres represent the Na^+ cations; the big green spheres are the Ba^{2+} cations. The planar nitrate species are represented in blue.

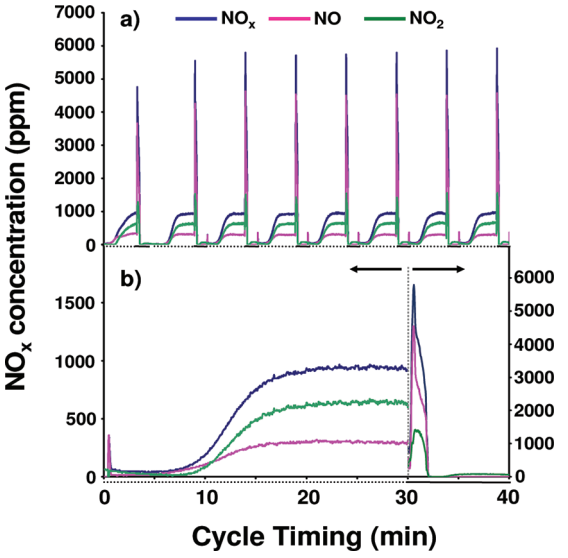

Figure 4. NO_x concentration traces at the adsorber outlet in a) cycles with 30 min adsorption (••••) and 10 min desorption (—) on a Ru(0.5%)/Ba,Na−Y zeolite at 300 °C. A detailed NO_x adsorption−desorption pattern one of these cycles is given in b). Adsorption gas was composed as 1000 ppm NO, 5% O_2, 3% H_2O and balance N_2. Regeneration of the adsorbent bed was done with 1% H_2, 3% H_2O and balance N_2.

resulting in corner-sharing sodium-water octahedra. After saturation with NO_x, electron density matching planar nitrate species was found between the Na^+ cations. The position suggested interaction with the zeolite framework via H-bonding (Figure 3).

Most surprisingly, no close contact between barium and NO_x species could be derived from the analysis of the structure. The obvious interaction between nitrate, sodium and the framework pinpointed the observed arrangement as a very stable situation of the nitrate species which explained why the regeneration of the adsorbent bed only occurred at high temperature.

To remedy the persistent formation of nitrate, we modified the material by introduction of ruthenium as yet a further cation in the framework. Previously, it was observed that the presence of Ru in Na−Y zeolite adsorbent led to a fast, reversible adsorption mechanism for NO_x.[18,19] During adsorption−desorption cycles, Ru inside the zeolite cavities reversibly changed oxidation state and position, generating and destroying the sodium-water networks in the pores which served as N_2O_3 adsorption site. Small amounts of metallic Ru on the outside of the zeolite crystals furthermore served as efficient oxidation catalyst converting part of the NO into NO_2. That information prompted analysis of the effect of Ru exchange into the above-described Ba,Na−Y in the hope that the expected different cation distribution prevented irreversible nitrate formation. Incorporation of even small amounts of Ru (0.5 wt %) into this zeolite system indeed led to a totally different and, most noteworthy, reversible NO_x adsorption behavior (Figure 4a). A representative NO_x adsorption−desorption cycle is shown in Figure 4b.

A significant NO_x uptake was observed during the first 10 min. Saturation was reached after 30 min. After saturation the main NO_x compound in the absorber outlet was NO_2, revealing the strong oxidation activity of the extra-zeolite ruthenium under oxidizing conditions. After switching to reducing conditions, regeneration of the adsorbent bed was completed after 3 min. The NO_x adsorption capacity was 10.1 ± 0.3 mg of NO_x/g. About half of the adsorbed NO_x was released as NO and NO_2. Formation of only negligible amounts of NH_3 and N_2O was detected, suggesting that a substantial part of the released NO_x was reduced by hydrogen to N_2. Increasing the Ru content to 1 and 3 wt % had no significant effect on the NO_x adsorption−desorption behavior nor the NO_x adsorption capacity. The NO/NO_2 ratio during the adsorption phase indicated that the iternal equilibrium was established by extra-zeolite ruthenium catalytic function.

H_2O was identified as a critical component in the gas stream, as in its absence no adsorption of NO_x occurred. ^{23}Na MAS NMR on Ru(3%)/Ba,Na−Y revealed water changed the local environment of sodium cations in the zeolite. Spectra of samples saturated with NO_x (Figure 5a) showed a single narrow Gaussian-like line around −22 ppm. After regeneration the signal broadened with a slight shoulder around −24 ppm (Figure 5b). Similar spectra had been observed earlier for the Ru/Na−Y zeolite.[18] The narrow line observed in the saturated sample corresponded to a symmetric environment of the Na^+ cations like in a well hydrated zeolite, where the cations do not directly interact with the framework.[17] The broadening and the expression of the shoulder was caused by changed electron density around some Na^+ nuclei after NO_x desorption. This typically is observed for partially dehydrated Na−Y zeolite with Na^+ preferentially occupying sites close to the framework of the host.[20,21]

Like for the analysis of the Ba,Na−Y zeolite, Rietveld analysis of powder X-ray diffraction data served to explore the structure of the Ru(0.5%)/Ba,Na−Y. According to XRD samples with a higher Ru content were found to contain significant amounts of

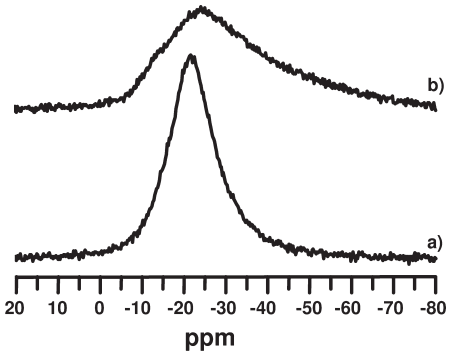

Figure 5. ^{23}Na MAS NMR spectra of a Ru(3%)/Ba,Na−Y zeolite (a) after NO_x adsorption and (b) after regeneration.

metallic Ru. Samples were taken after NO_x saturation and after regeneration at 300 °C in the reactor. The unit cell composition was determined via ICP-AES and corresponded to $Ru_{0.7}Ba_{17}Na_{15.8}Al_{52}Si_{140}O_{384}$. The amount of water molecules freely refined by Rietveld refinement corresponded well with the experimentally determined value obtained by TGA (see ESI). Like in absence of ruthenium (Figure.2), during the NO_x adsorption phase Ba^{2+} cations were found on position SI′ and SII* in, and close to the sodalite cages. This again forced the Na^+ cations to take positions in the supercages on positions SIII and SV. However, the presence of Ru in the sample caused fewer SI′ positions to be occupied by Ba^{2+} compared to the Ba,Na−Y zeolite. This allowed Na^+ cations to access some few SII* positions. This way, construction of a complex water−sodium network involving SII*, SIII and SV Na^+ cations in the supercages was possible. The organization of the Na^+ cations and water molecules in the supercages was very similar to what was found in barium-free Na−Y and Ru/Na−Y zeolites.[5,17,18] However, the SII−SIII−SV clusters with highly symmetric, octahedral Na^+ environments were less extended and more strongly branched at the SV cations. Position and occupation of the water positions clearly indicated no extended chains of SIII and SV cations occurred in this sample. Electron density between an SV, SIII and SII Na^+ ion was assigned to adsorbed N_2O_3, replacing H_2O molecules and bridging SV,SIII and SII* octahedra (Figure 6). Similar as in Ru/Na−Y, position SI in the hexagonal prism was found occupied, most probably by Ru^{3+}. During regeneration these Ru^{3+} cations were reduced to Ru° and moved from cation position SI to cation position SU in the center of the sodalite cage.[17,18] This changed the charge distribution and caused the sodium ions on SIII to shift closer to the framework, therewith disrupting the water-network necessary for NO_x adsorption and causing a rapid release of the adsorbed NO_x.

The observation of clustered sodium-water networks suggested that occupation of all potential adsorption sites by N_2O_3 might have been hindered. Therefore, the effect of further diluting the sodium ions by increasing the barium content was explored. To study this effect the concentration of Ba was increased by an additional ion exchange from 67% to 90% of the cation exchange capacity. Before the second ion exchange the Ba,Na−Y zeolite was first calcined at 500 °C for 4 h. Elemental analysis resulted in a unit cell composition of $Ba_{23.5}Na_{5.0}Al_{52}Si_{140}O_{384}$. The zeolite was further exchanged with 0.5 wt % Ru resulting in a unit cell composition of $Ru_{0.76}Ba_{22.8}Na_{4.0}Al_{52}Si_{140}O_{384}$. As before, NO_x adsorption−desorption cycles were performed following the standard procedure with 1000 ppm NO.

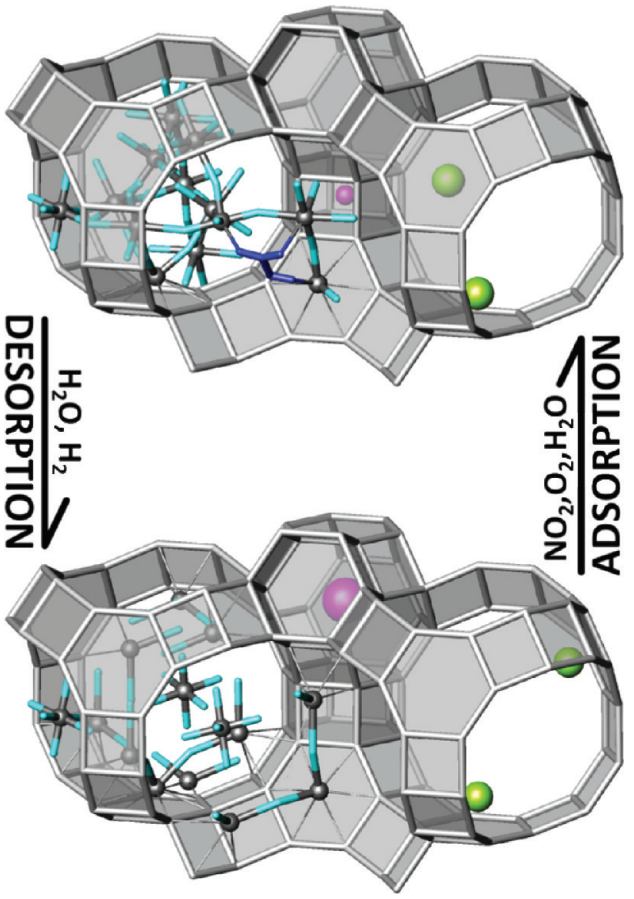

Figure 6. Representation of the NO_x adsorption−desorption mechanism of a Ru(0.5%)/Ba,Na−Y zeolite (15.8 Na^+ per unit cell) during oxidative−reductive NO adsorption−desorption cycles based on Rietveld refinement. The Na^+ cations are represented as the gray spheres, the Ba^{2+} cations on SII' sites as the green spheres and the Ru^{3+} atom is shown as the purple sphere. The adsorption of NO_x as N_2O_3 during lean phase is represented as the blue molecules.

During the first 15 min of the adsorption phase, a significantly improved NO_x uptake was observed. Saturation of the adsorbent was reached after 30 min exposure to 1000 ppm NO and regeneration was complete after 3 min. The NO_x adsorption−desorption behavior was similar to Ru(0.5%)/Ba,Na−Y with lower Ba content. However, the NO_x adsorption capacity significantly increased to 16.1 ± 0.4 mg NO_x/g. Such a strong positive effect was rather surprising, as the NO_x adsorption was associated with the presence of sodium on specific cation sites. The amount of Na^+ cations in the Ru(0.5%)/Ba,Na−Y zeolite was drastically decreased by the second Ba exchange. It appeared strange such a small amount of Na^+ cations could offer so many NO_x adsorption sites to explain the high capacity. However, a similar NO_x adsorption−desorption behavior pointed at a similar NO_x adsorption mechanism even though only few sodium ions remained in the structure. As before, Rietveld refinement was applied to analyze the structure of the adsorbent. The same positions for Na^+ and Ba^{2+} were found in the structure but massive extra electron density on position SII′ was also observed. Assuming this position to be occupied by Ba^{2+}, refinement of the occupation numbers on SII*, SII′, and SI′ yielded the correct number of Ba^{2+} per unit cell. Refinement of Na^+ occupation on SV and SIII resulted in one and two Na^+, respectively. The occupation of Na^+

dx.doi.org/10.1021/cm202230r |Chem. Mater. 2011, 23, 4606–4611

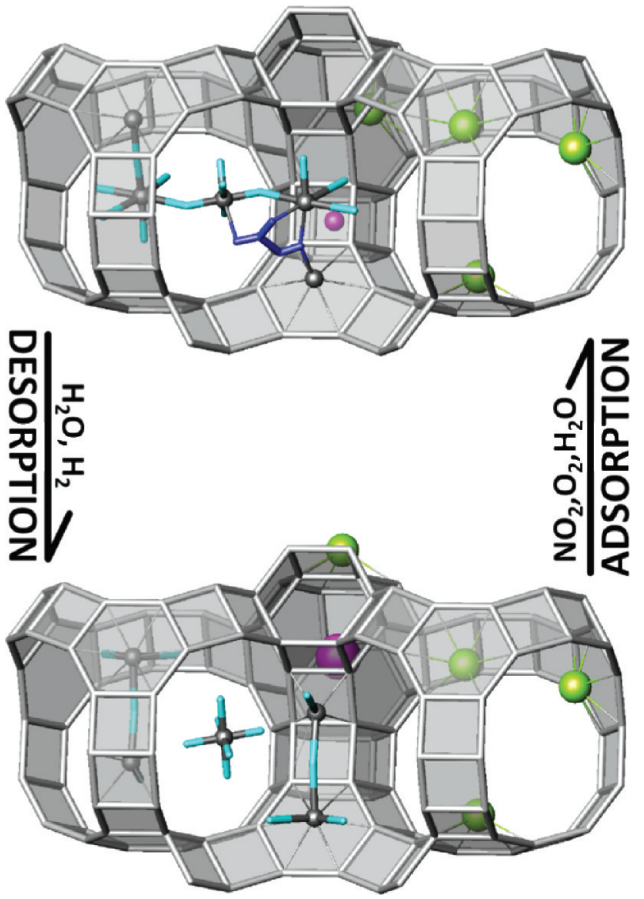

Figure 7. Representation of the NO_x adsorption−desorption mechanism of a Ru(0.5%)/Ba,Na−Y zeolite (4 Na^+ cations per unit cell) during NO adsorption−desorption cycles at 300 °C based on Rietveld refinement. The zeolite was 2 times exchanged with Ba. The adsorption of NO_x as N_2O_3 during lean phase is represented as the blue molecule. The Na^+ cations are represented as the gray spheres which coordinate the N_2O_3 molecule. Ba^{2+} cations represented by green spheres populate SII' sites on walls of supercages. The Ru^{3+} atom is shown as the purple sphere.

on SII* was at first fixed to two Na^+ next to Ba^{2+} and proved stable, later in the refinement. Despite the very low occupation numbers of water, refinement of their position was attempted. The best results were obtained by 3 corner sharing octahedra of Na^+ on SIII−SV−SIII, with each SIII linked to one SII* position (Figure 7).

Compared to the earlier reported corresponding structure in Ru,Na−Y[18] this fragment of the water network appeared more flexible because octahedra around the SIII ions were no longer fixed by interaction with two SV positions. Introduction of N_2O_3 molecules as rigid bodies into the refinement resulted in a very satisfactory fit of the powder pattern so that the adsorption of 2 N_2O_3 molecules, one on each side of the SV ion appeared feasible (Figure 7). This occupation was in full agreement with the measured capacity of the material. It seemed that by heavily fragmenting the sodium water networks their accessibility and affinity for N_2O_3 is increased so that optimum loading of these sites can occur in the twice Ba-exchanged zeolite.

In summary, the incorporation of Ru into Ba,Na−Y led to a different NO_x adsorption behavior/mechanism compared to the nitrate formation in Ba,Na−Y zeolite. This was caused by equilibration of NO and NO_2 by the Ru phase outside the zeolite[17,18]

Table 1. Overview of Used Adsorbents

catalyst	feed (ppm)	NO_x sorbed (mg/g)	reversible
Ru(3%)Na−Y[a]	NO/1000	3.2	yes
Ru(1%)Na−Y	NO/ 1000 ppm	4.8	yes
BaNa-Y	NO_2/ 1500 ppm	20.95	no
Ru(0,5%)Ba,Na−Y	NO/ 1000 ppm	10.1	yes
Ru(0,5%)Ba,Na−Y[a]	NO/ 1000 ppm	16.1	yes

[a] Double ion exchange of Ba^{2+} .

and by Ru atoms in the zeolite which directly influenced occupation of cation positions in the sodalite cages and the supercages. In absence of Ru, Na^+ cations preferred positions SIII and SV in the supercages of the zeolite. Between these cations, planar nitrate species adsorbed at a stable position. Regeneration of a saturated adsorbent bed only occurred at high temperature (Figure 2). In presence of Ru, some Na^+ cations could occupy position SII* besides SIII and SV. This occupation allowed formation of a H_2O network, linking the Na^+ cations in the supercages via water molecules. N_2O_3 molecules could adsorb in this H_2O−Na^+ network competing with the H_2O molecules. The reduction and replacement of Ru during regeneration shuffled the cation positions: Na^+ cations moved closer to the framework giving them a more asymmetric coordination as seen from the ^{23}Na MAS NMR spectrum of the Ru/Ba,Na−Y zeolite after regeneration. Only a small amount of Ru was required to obtain this reversible NO_x adsorption−desorption behavior. Increasing the amount of Ba^{2+} cations in the Ru zeolite, led to further increase of the NO_x adsorption capacity. The reduced number of sodium cations resulted in a severely fragmented Na^+-H_2O network with higher accessibility and presumably higher flexibility increasing significantly the capacity of the adsorbent.

A summary of all tested catalysts can be found in Table 1. The introduction of Ru in the Na−Y zeolite has been shown to cause a remarkable reversible NO_x adsorption/desorption behavior of NO containing feed with NO_x adsorbed as N_2O_3. Compared to the maximum NO_x uptake of the Ru(1%)/Na−Y zeolite (4.8 ± 0.1 mg of NO_x/g) and single Ba-exchanged Ru(0.5%)/Ba,Na−Y (10.1 ± 0.1 mg of NO_x/g)) the capacity in the twice Ba-exchanged material has tripled (16.1 ± 0.4 mg of NO_x/g) while the mechanism still is reversible and release easily could be triggered by switching to reducing conditions.

CONCLUSIONS

Ru/Ba,Na−Y zeolite was identified as a reversible NO_x adsorbent. NO_x is adsorbed as N_2O_3 in the supercages of the faujasite zeolite. Compared to the earlier discovered Ru/Na−Y zeolite the introduction of barium leads to a 3-fold increase of the NO_x adsorption capacity, whereas the state of adsorbed NO_x remains the same. It is expected that in an eventual application of Ru/Ba,Na−Y adsorbent the regeneration could effectively be controlled by the lean-rich management of the engine. The concentrated NO_x stream desorbing from the Ru/Ba,Na−Y zeolite trap may be eliminated using a periodic NO_x recirculation system[22] or a downstream SCR catalyst.[23] Asides the clear potential for application of the studied system it also taught that detailed understanding of the synergy between zeolite framework, cations and guest molecules can lead to astonishing new functionalities.

■ ASSOCIATED CONTENT

Supporting Information. More information concerning the strategy of Rietveld refinement and thermogravimetric data; CIF files of the refined powder data have also been deposited at the ICSD with CSD numbers 422294−422298. This material is available free of charge via the Internet at http://pubs.acs.org.

■ AUTHOR INFORMATION

Corresponding Author

*Fax: (+32) 1632-1998. E-mail: christine.kirschhock@biw.kuleuven.be.

Author Contributions

‡Sylvia Smeekens and Steven Heylen contributed equally.

■ ACKNOWLEDGMENT

J.A.M. and C.E.A.K. acknowledge the Flemish Government for long-term structural funding (Methusalem). The work is part of a concerted research action (GOA) and supported by Excellence funding (CECAT). S.H. acknowledges the Flemish FWO for a PhD grant.

■ REFERENCES

(1) Sedlmair, C.; Seshan, K.; Jentys, A.; Lercher, J. A. *J. Catal.* **2003**, *214*, 308.
(2) Mahzoul, H.; Brilhac, J. F.; Gilot, P. *Appl. Catal., B* **1999**, *20*, 47.
(3) Lietti, L.; Forzatti, P.; Nova, I.; Tronconi, E. *J. Catal.* **2001**, *204*, 175.
(4) Lesage, T.; Verrier, C.; Bazin, P.; Saussey, J.; Daturi, M. *Phys. Chem. Chem. Phys.* **2003**, *5*, 4435.
(5) Sultana, A.; Loenders, R.; Monticelli, O.; Kirschhock, C. E. A.; Jacobs, P. A.; Martens, J. A. *Angew. Chem.* **2000**, *112*, 3062. *Angew. Chem., Int. Ed.* **2000**, *39*, 2934.
(6) Bentrup, U.; Brückner, A.; Richter, M.; Fricke, R. *Appl. Catal., B* **2001**, *32*, 229.
(7) Brosius, R.; Martens, J. A. *Top. Catal.* **2004**, *28*, 119.
(8) Kwak, J. H.; Szanyi, J.; Peden, C. H. F. *Catal. Today* **2004**, *89*, 135.
(9) Kwak, J. H.; Szanyi, J.; Peden, C. H. F. *J. Catal.* **2003**, *220*, 291.
(10) Wen, B.; Yeom, Y. H.; Weitz, E.; Sachtler, W. M. H. *Appl. Catal., B* **2004**, *48*, 125.
(11) Yeom, Y. H.; Wen, B.; Sachtler, W. M. H.; Weitz, E. *J. Phys. Chem. B* **2004**, *108*, 5386.
(12) Sung, C.-Y.; Broadbelt, L. J.; Snurr, R. Q. *Catal. Today* **2008**, *136*, 64.
(13) Sung, C.-Y.; Snurr, R. Q.; Broadbelt, L. J. *J. Phys. Chem. A* **2009**, *113*, 6730.
(14) Szanyi, J.; Kwak, J. H.; Peden, C. H. F. *J. Phys. Chem. B* **2004**, *108*, 3746.
(15) Szanyi, J.; Kwak, J. H.; Burton, S.; Rodriguez, J. A.; Peden, C. H. F. *J. Electron Spectrosc. Relat. Phenom.* **2006**, *150*, 164.
(16) Monticelli, O.; Loenders, R.; Jacobs, P. A.; Martens, J. A. *Appl. Catal., B* **1999**, *21*, 215.
(17) Mortier, W. J. *Compilation of Extra Framework Sites in Zeolites*; Butterworth Sci. Ltd.: Guildford, U.K., 1982.
(18) Smeekens, S.; Heylen, S.; Villani, K.; Houthoofd, K.; Godard, E.; Tromp, M.; Seo, M.; DeMarco, M.; Kirschhock, C. E. A.; Martens, J. A. *Chem. Sci.* **2010**, *1*, 763.
(19) Labaki, M.; Issa, M.; Smeekens, S.; Heylen, S.; Kirschhock, C. E. A.; Villani, K.; Jeguirim, M.; Habermacher, D.; Brilhac, J. F.; Martens, J. A. *Appl. Catal., B* **2010**, *97*, 13.
(20) Hu, K.-N.; Hwang, L.-P. *Solid State Nucl. Magn. Reson.* **1998**, *12*, 211.
(21) Engelhardt, G.; Hunger, M.; Koller, H.; Weitkamp, J. *Studies in Surface Science and Cataysis*; Weitkamp, J., Karge, H. G., Pfeifer, H., Hölderich, W., Eds.; Elsevier: Amsterdam, The Netherlands, 1994; Vol. 84.
(22) Chaize, E.; Webster, D. E.; Krutzsch, B.; Wenninger, G.; Weibel, M.; Hodjati, Sh.; Petit, C.; Pitchon, V.; Kiennemann, A.; Loenders, R.; Monticelli, O.; Jacobs, P. A.; Martens, J. A.; Kasemo, B. SAE982593 1998.
(23) Zukerman, R.; Vradman, L.; Herskowitz, M.; Liverts, E.; Liverts, M.; Massner, A.; Weibel, M.; Brilhac, J. F.; Blakeman, P. G.; Peace, L. G. *Chem. Eng. J.* **2009**, *155*, 419.